Published in final edited form as:
Eur J Neurosci. 2013 December ; 38(12): . doi:10.1111/ejn.12351.

Microarray assisted fine mapping of quantitative trait loci on Chromosome 15 for susceptibility to seizure-induced cell death in mice

P. Elyse Schauwecker
Department of Cell and Neurobiology, USC Keck School of Medicine, Los Angeles, CA 90033

Abstract

Prior studies with crosses of the FVB/NJ (FVB; seizure-induced cell death susceptible) mouse and the seizure-induced cell death resistant mouse, C57BL/6J (B6), revealed the presence of a quantitative trait locus (QTL) on chromosome 15 (Chr. 15) that influenced susceptibility to kainic acid-induced cell death (*Sicd2*). In an earlier study, we confirmed that the *Sicd2* interval harbors gene(s) conferring strong protection against seizure-induced cell death through the creation of the FVB.B6-*Sicd2* congenic strain and created three interval-specific congenic lines (ISCLs) that encompass *Sicd2* on Chr. 15 to fine-map this locus. To further localize this *Sicd2* QTL, an additional congenic line carrying overlapping intervals of the B6 segment was created (ISCL-4) and compared to previously created ISCLs-1-3 and assessed for seizure-induced cell death phenotype. While all of the ISCLs exhibited reduced cell death associated with the B6 phenotype, the most dramatic of these, ISCL-4 showed the most extensive reduction in seizure-induced cell death throughout all hippocampal subfields. In order to characterize the susceptibility loci on *Sicd2* using this ISCL and identify compelling candidate genes, we have undertaken an integrative genomic strategy of comparing exon transcript abundance in the hippocampus of this newly developed Chr. 15 subcongenic line (ISCL-4) and FVB-like littermates. We identified ten putative candidate genes that are alternatively spliced between the strains and may govern strain-dependent differences in susceptibility to seizure-induced excitotoxic cell death. These results illustrate the importance of identifying transcriptomics variants in expression studies, and implicate novel candidate genes conferring susceptibility to seizure-induced cell death.

Keywords

Enpp2; Oxr1; Rspo2; Trhr; hippocampus; subinterval congenics; transcriptome profiling

Introduction

It is clear from a number of investigations that dramatic variation in susceptibility to seizure-induced cell death exists among various mouse stocks and strains and that genetic factors play an important role in determining susceptibility to seizure-induced excitotoxic cell death (Schauwecker & Steward, 1997; McKhann *et al.*, 2003; Schauwecker *et al.*, 2004; McLin & Steward, 2006; Winawer *et al.*, 2007; Müller *et al.*, 2009). We have found that susceptibility to seizure-induced excitotoxic cell death occurs in many inbred strains of mice and often differs in extent among strains due to genetic background. In particular, FVB/NJ (FVB) mice experience significantly more seizure-induced cell death than C57BL/6J (B6). This differential sensitivity is explained by genes present in quantitative trait loci (QTL).

Corresponding author: P. Elyse Schauwecker, Ph.D., Dept of Cell and Neurobiology, USC Keck School of Medicine, 1333 San Pablo Street, BMT 403, Los Angeles, CA 90033, Tel: (323) 442-2116, Fax: (323) 442-2411, schauwec@usc.edu.

Previously, linkage studies using (C57BL/6J X FVB/NJ)N2 mice mapped three susceptibility loci for the trait of seizure-induced excitotoxic cell death to chromosomes (Chrs.) 18, 15, and 4 (listed in order of strength of influence on the phenotype) and designated *Sicd*, for seizure-induced cell death (Schauwecker *et al.*, 2004). The three significant QTLs (Chrs 4, 15, 18) together account for nearly 25% of the trait variance for both genders combined (Schauwecker *et al.*, 2004). Subsequently, through the development of the congenic strain, FVB.B6-*Sicd2*, we were able to confirm that the *Sicd2* interval on Chr. 15 harbors gene(s) conferring strong protection against seizure-induced excitotoxic cell death (Schauwecker, 2011). Interval-specific congenic lines (ISCLs) that encompass *Sicd2* on Chr. 15 were generated and used to fine-map this QTL to a 21.16 Mb interval containing approximately 169 known or predicted genes (Schauwecker, 2011).

However, we were interested in further refining this candidate region to enable rational candidate gene approaches toward the identification of the underlying genes. In the present study, we carried out a study of a subcongenic Chr. 15 *Sicd2* QTL and FVB-like littermates using Affymetrix GeneChip Mouse Exon 1.0 ST arrays to assess exon- and gene-level expression differences in ex vivo hippocampal cells. It is known that many genes underlying a variety of phenotypes show significant expression level variations in relevant tissues across genetically segregating populations, and transcriptional regulation of these genes may play an important role in phenotype manifestation. Upstream regulators (transcription factors, signaling molecules, etc.) of these genes are likely to be the genetic drivers of the corresponding phenotypes as well. Therefore, investigations on expression profiles on the transcriptome level can help greatly in gaining a better understanding of molecular disturbances in disease. As a result, a microarray application to discovering *Sicd* QTLs could provide a shortcut to directly and rapidly identify gene candidates with expression differences. Here, we identified ten genes that are alternatively spliced between the strains and may govern strain-dependent differences in susceptibility to seizure-induced cell death.

Materials and methods

This study was carried out in strict accordance with the recommendations in the Guide for the Care and Use of Laboratory Animals of the National Institutes of Health. The protocol was approved by the USC Animal Care and Use Committee (Protocol #:11638). All efforts were made to minimize the number and suffering of any animals used in these experiments.

Development of interval-specific congenic lines for fine-mapping and progeny testing

The series of ISCL1-4 were developed and bred in our colony at the Zilkha Neurogenetic Institute at the University of Southern California Keck School of Medicine as previously reported (Schauwecker, 2011). In summary, individual congenic recombinant mice (FVB.B6-*Sicd2*) were backcrossed to FVB mice (purchased from Jackson Laboratories, Bar Harbor, ME, USA), resulting in multiple offspring with the same recombination (also referred to as an ISCL). Individual progeny were genotyped using six microsatellite markers within or flanking the *Sicd2* QTL to identify recombinant mice and define the boundaries of the introgressed region. At the same time that recombinations in the previous generation were being replicated, additional recombinants were sought in four subsequent backcross generations in an ever-narrowing QTL interval and replicated as needed. These mice were heterozygous for a reduced B6 interval and were then brother-sister mated to produce a first round of congenics. Heterozygote mating was used to perpetuate the ISCL lines and to create FVB-like littermate controls (homozygous for FVB alleles across the subcongenic interval) for comparison. No genotyping, other than on the B6 interval, was done in the ISCLs as the backcross was always to FVB. All ISCLs were backcrossed for >6 generations prior to experiments.

DNA isolation and microsatellite genotyping

High-molecular weight mouse tail DNA was used as a template for PCRs and genomic DNA was extracted from the tail of the animal according to a previously published protocol (Miller *et al.*, 1988). Briefly, a small piece (~1 cm) of the tip of the tail was cut off using sharp scissors. Tail tips were incubated overnight at 55°C in 635 μl of lysis solution containing 600 μl Tris-NaCl-ethylenediaminetetraacetic acid (EDTA)-sodium dodecyl sulfate (SDS) buffer (10 mM Tris, pH 7.5, 400 mM NaCl, 100 mM EDTA and 0.6% SDS) and 35 μl proteinase K (10 mg/ml). DNA was isolated using a high-salt method and standard procedures of ethanol precipitation and resuspension in Tris-EDTA (10 mM Tris, 1 mM Na_2-EDTA, pH 7.4) and storage at 4°C. After redissolving the DNA, DNA concentrations were determined spectrophotometrically and samples diluted to 100 ng/μl.

Microsatellite genotyping was conducted as previously described (Schauwecker *et al.*, 2004). In brief, microsatellite primers were purchased from Invitrogen (Carlsbad, CA, USA). Primers were selected based on their map locations and on their being polymorphic between parental strains (http://www.genome.mit.edu). After a 3-min incubation at 94°C, the reactions were amplified through 35 cycles of 30 seconds at 94°C, 60 seconds at 55°C and 45 seconds at 72°C, followed by 10 min at 72°C. For markers with allele differences of 8 bp or greater, we used a non-isotopic method of analysis involving sizing of the PCR products by loading them onto 4% agarose gels (Genepure HiRes Agarose, ISC Bioexpress, Kaysville, UT, USA) and visualizing them with ethidium bromide staining of PCR products. After electrophoresis, two independent scorers recorded genotypes from gels analyzed with a digital gel documentation system (Gel-DocIt, UVP, Upland, CA, USA) that provides digital images from ethidium bromide-stained gels. To minimize genotyping errors, any discrepancies or inconsistencies in genotype readings were resolved either by retyping or discarding questionable genotypes. The map positions of the microsatellite markers and genes were derived from either the December 2011 (NCBI Build m38) release of the Mouse Genome Sequencing Consortium (http://www.genome.ucsc.edu/) or its megabase position from the Mouse Genome Database (http://www.informatics.jax.org/ April 2013).

Systemic kainate administration

The phenotypic effects of the *Sicd2* region in ISCLs 1–4 were assessed by progeny testing (Darvasi, 1997, 1998) by comparing the phenotype of mice homozygous for the recombinant chromosome with that of FVB-like littermates. Identification of the ISCLs that show a QTL effect on the phenotype of susceptibility and the ISCLs that do not show a QTL effect on the phenotype of susceptibility defined the critical genomic interval required for the QTL effect.

Young adult mice, 6–8 weeks old, (ISCLs1-4, and FVB-like littermates) were administered kainic acid (Nanocs, New York, NY, USA), dissolved in isotonic saline (pH 7.3) and at a dose of 20 mg/kg (s.c.). To minimize mortality following status epilepticus (SE) because of dehydration or starvation, animals were fed moist high-fat rodent chow until animals were observed to be eating dry chow. In our experience, 20% of mice die during SE at this dose of kainate. The mortality is not line/strain or seizure intensity dependent and all deaths tended to occur during the 4 hour observation period.

Behavioral assessment of kainate-induced seizures

Mice were monitored continuously for 4 hours for the onset and extent of seizure activity using a previously defined six-point seizure scoring scale (Schauwecker & Steward, 1997) that was adapted from a five-point scale for rats (Racine, 1972). The behavioral progression of KA-induced seizures was rated and recorded as follows: Stage 1, immobility; Stage 2, forelimb and/or tail extension, rigid posture; Stage 3, repetitive movements, head bobbing;

Stage 4, rearing and falling; Stage 5, continuous rearing and falling; and Stage 6, severe tonic-clonic seizures. SE was defined as continuous behavioral seizure activity that lasted for at least 30 min or a series of intermittent seizures without restoration of normal behavioral patterns between successive seizures. The severity of SE was evaluated by the percentage of time that animals spent in stage 4/5 seizures during SE. For mice to be included in the study, they had to exhibit at least 45 min of continuous stage 4/5 seizures, as previous studies have suggested that there is a direct relationship between the generation of epileptiform activity and the extent of damage in hippocampal subfields (Sperk *et al.*, 1983; Ben-Ari, 1985; Sperk, 1994). Seizure parameters monitored included latency of convulsions and duration of severe (Stage 4/5) seizure activity. All experiments were approved by the Institutional Animal Care and Use Committee (IACUC) of the University of Southern California and conducted in accordance with its guidelines. Every effort was made to minimize animal suffering and to minimize the number of animals utilized in order to produce reliable scientific data.

Tissue preparation and histological staining

To evaluate the severity of brain damage associated with seizures, brains from animals of each strain were processed for cresyl violet staining to assess cell loss and morphology according to previously published methods (Schauwecker *et al.*, 2004; Lorenzana *et al.*, 2007). Briefly, seven days following kainate administration, mice were anesthetized and transcardially perfused with 4% paraformaldehyde in 0.1M phosphate buffer (pH 7.4). Brains were removed and post-fixed overnight. Brains were left in 30% sucrose for at least 12–18 hours for cryoprotection. Horizontal (40 μm) frozen sections were be cut on a sliding microtome and immersed in 0.1M phosphate buffer (pH 7.4) free-floating, until histological processing had begun. Every sixth section (~240 μm) was processed for cresyl violet staining to assess cell loss and morphology.

NeuN immunofluorescence

Immunofluorescence was performed on an additional series of sections (every sixth section; ~240 μm) to detect those neurons that survived 7 days following kainate-induced SE. For immunofluorescent labeling, sections were washed with 0.1M phosphate buffer (pH 7.4) and blocked with 5% normal serum and 0.1% Triton X-100 in 0.1M phosphate buffer (pH 7.4). Next, sections were incubated overnight with a neuronal marker against NeuN (monoclonal from mouse; Millipore, Billarica, MA, USA; 1:500) at 4°C. After several washes, sections were incubated with a secondary antibody from mouse conjugated with Cy2 (1:200; Jackson Immuno- Research, West Grove, PA, USA) for 2 h at room temperature. After rinsing, sections were mounted and coverslipped with ProLong anti-fade mounting medium (Molecular Probes, Eugene, OR, USA). For labeling, omission of the primary antibody served as negative control for staining in which the tissue was incubated with antibody diluent, without the primary antibody included. Labeling for NeuN was viewed under an Olympus BX51 fluorescence microscope (Olympus, New York, NY, USA).

Morphological assessment of neuronal damage

To provide a global picture of genotype-dependent effects on cell loss throughout the hippocampus, neuronal degeneration was evaluated in sections stained with cresyl violet. The number of degenerating neurons in both the right and the left hippocampus from every sixth section (240 μm separation distance) in four brain regions (CA3, CA1, dentate hilus, and dentate gyrus), which represented various levels of the hippocampus, was visually estimated and a histological damage score was assigned on a 0–3 grading scale and according to the following criteria: grade 0, absence of pyknotic cells; grade 1.0, mild (<25% of cell pyknotic); grade 2.0, moderate (<50% of hippocampal neurons pyknotic) and

grade 3.0, extensive (>50% of cells pyknotic) according to previously defined scale (Fujikawa *et al.*, 1994; Fujikawa, 1995, 1996; Schauwecker *et al.*, 2004). All grading was performed blindly by an observer who was naïve to the strain.

There was no obvious difference in neuronal damage between hemispheres, so values for right and left hemispheres were averaged for each mouse. For the hippocampus, scores from sections were averaged and used for calculating group values. As histological damage scores were normally distributed, we were able to use standard parametric methods of data analysis. Thus, to determine whether differences in histological scores existed among the groups of mice, results were assessed statistically by one-way Analysis of Variance (ANOVA) with the computer program SigmaStat version 3.50 (Jandel Scientific, San Rafael, CA, USA) and intergroup differences were analyzed by Student Newman-Keuls *post hoc* test.

Quantitative analysis of seizure-induced cell loss

Subsequently, to determine the susceptibility of individual hippocampal subfields to neurotoxic insult, we counted neurons in cresyl violet-stained sections. Quantitative analysis of hippocampal cell counts was performed by an observer blinded to the strain groups using unbiased stereological methods as described previously (Lorenzana *et al.*, 2007; Kong *et al.*, 2008). The cresyl violet-stained neurons in area CA3, area CA1, the dentate hilus, and the dentate gyrus were counted in both the right and left hippocampus and counting was initiated within the ventral hippocampus at the first point where hippocampal subfields could be easily identified. This level corresponded to horizontal section 54, based on the atlas of Sidman *et al.* (1971). Hippocampal subfields were based on Franklin & Paxinos (1997) classification and discrimination between the CA3 and the dentate hilus region was based on morphological features and locations of the cells (West *et al.*, 1991; Sousa *et al.*, 1998). Specifically, for dentate hilar cell counts, the hilus was operationally defined as the region bordered by the supra- and infrapyramidal granule cell layers and excluding the densely packed pyramidal neurons of area CA3. Neuron counts were made in all subfields and the numbers for each side were averaged into single values for each animal. Surviving cells were counted only if they were contained within the pyramidal cell layer, dentate hilus or dentate gyrus possessed a visible nucleus and characteristic neuronal morphology and had a cell body larger than 10 μm. Six square counting frames (200 × 200 μm) were randomly placed in the pyramidal layer of fields CA1 and CA3 or in the dentate gyrus in 4–5 regularly spaced horizontal sections from each animal. Two square counting frames were randomly placed in the dentate hilus in 4–5 regularly spaced horizontal sections from each animal. Neuronal nuclei were evaluated at three different focal planes and only those in the focal plane were counted with a 40X objective and considered as a counting unit. Stereological analysis was performed with the aid of ImagePro Plus 4.5 software (Media Cybernetics, Silver Spring, MD, USA) and a motorized Z-stage (Optiscan; Prior Scientific, Fairfax, VA, USA). Final cell counts were expressed as the percentage of cells as compared to saline-injected sham control FVB-like littermates. Results were assessed statistically by one-way analysis of variance (ANOVA) using the computer program, SigmaStat (Jandel Scientific, San Rafael, CA, USA), and intergroup differences were analyzed by Newman-Keuls *post hoc* test.

RNA isolation

For RNA isolation, naïve mice were anesthetized with Avertin and killed by decapitation. Whole brains were removed by dissection and both hippocampi rapidly dissected out on ice. Both combined hippocampi from a mouse whole brain (~50 mg) were homogenized and total RNA extracted using the RiboPure kit™ (Ambion, Austin, TX, USA) following manufacturer's protocols. RNA concentration was determined using a Molecular Devices

SpectraMax 190 spectrophotometer (Molecular Devices, Sunnyvale, CA, USA), and integrity was evaluated using the Bioanalyzer 2100 platform (Agilent Technologies, Santa Clara, CA, USA). RNA samples were stored at −80°C until analyzed.

RNA labeling and microarray hybridization

10–20 μg of total RNA was mixed with 200 pMol of oligo-dT primer. After a 10 min incubation at 70°C and 5 min at 4°C, 20 units of Transcriptor reverse transcriptase (Roche, Palo Alto, CA, USA), 10 nMol of each dNTP and 4 nMol of aminoallyl-dUTP (Ambion, Austin, TX, USA) was added and this mix was incubated 2 hours at 42°C. After 30 min of RNase treatment, cDNA was purified using QIAquick PCR purification kits (Qiagen, Valencia, CA, USA). The amount of cDNA was determined spectrophotometrically, and samples were dried in a speedvac. cDNA was resuspended in a carbonate buffer (pH 9.0–9.3) and mixed with the Cy3- and Cy5-NHS ethers (Amersham, Piscataway, NJ, USA). After a 1 hour incubation in the dark, 20 mMol of hydroxylamine was added to quench the reaction, and labeled cDNA were purified using QIAquick PCR purification kits. The concentration of the labeled cDNA and labeling efficiency were determined spectrophotometrically, and labeled cDNA was hybridized to Affymetrix Mouse Exon 1.0 ST microarrays according to manufacturer's instructions.

Microarray experiments, including generation of probes, hybridization to arrays, washing and scanning, were conducted at the University of Tennessee DNA and Microarray Core Facility using Affymetrix Mouse Exon 1.0 ST microarrays on a fee-per-service basis. We used the Affymetrix Mouse Exon 1.0 ST microarray, which carries 1.2 million probe sets covering one million exon clusters, with an average of 40 probes per gene. All-exon arrays provided an opportunity to measure both gene expression and alternative RNA splicing. Unlike the conventional 3′ arrays, transcript-level changes in expression are determined by calculating the mean change in all the exons in a transcript cluster. In addition to transcript-level changes, the new all-exon arrays can measure changes in alternative splicing, by following the expression of each exon, or probeset, independently. Exon arrays are a high-density microarray platform with probes designed to target all annotated and predicted exons in the genome. A probeset, consisting of four probes, is designed to target a single putative exonic region. Furthermore, each exonic region is classified based on the supporting type of annotation. In addition to probes targeting each exon supported by RefSeq mRNA evidence (core probes), Exon arrays also have probes that target exons supported solely by expressed sequence tag evidence (extended probes) or by purely computational predictions (full probes).

Bioinformatic analysis using Partek® Genomics Suite™

Normalized microarray data were retrieved from the University of Tennessee DNA and Microarray Core Facility and imported into Partek® Genomics Suite™ 6.6 (Partek, Missouri, USA) to assess the quality of the data and perform statistical analyses. Affymetrix CEL files were imported using the Robust Multi-Chip Average (RMA) algorithm. Affymetrix library files used in conjunction with Partek® Genomics Suite™ were the V1 release version for the Mouse Exon 1.0 ST Array, and annotation files were from NetAffx (www.affymetrix.com). Core probesets only were selected and a gene-level summary analysis was conducted. All files were loaded to conduct analyses of all samples, and all samples were normalized before conducting hierarchical clustering analyses. Data filtration is required to decrease the chances of false predictions, therefore, increasing the verification rate. Pre-analysis filtration included removing any probe set that is not expressed in at least one sample group. The data analysis workflow for exon arrays was two pronged. For determination of differential expression, probe set information was summarized into gene level information. Using the Partek "gene expression workflow" to detect differentially

expressed genes, an ANOVA was performed. ANOVA factors included chip number and line. Data were filtered to include only data points that had a detection p-value less than 0.05 and a fold-change cut-off of 1.2 in all analyses to minimize the risk of generating false positive results. Gene expression differences between the ISCL and FVB-like littermates were determined using a false discovery rate (FDR) of 0.05 in a step up analysis. From this analysis, gene lists were created and exported lists included significant genes, fold changes and p-values for comparisons between groups. To identify candidate quantitative trait genes (QTGs), we filtered for genes that map to our reduced region on chromosome 15 and that showed significant changes in transcript levels based on the ANOVA Bonferroni algorithm using a cutoff P value of 0.05.

A second analysis looked at exon level data. In order to obtain meaningful alternate exon usage information, and to decrease the chance of false positives, several filtering steps were included prior to analysis. The presence of absence of exon expression was determined using detection above background (DABG). All probe sets where the DABG p-value <0.05 were removed from the analysis. Data were analyzed for alternative splicing by an ANOVA with Strain as the main effect and corresponding interaction.

All exon array data were analyzed using tools in Genomics Suite software (v6.6; Partek Inc., St. Louis, MO, USA), using Affymetrix annotation files (NetAffx, www.Affymetrix.com). Exon level data were filtered to include only those probe sets that are in the “core” meta-probe list, which represents 17,881 RefSeq genes and full-length GenBank mRNAs. The core data include target-sequence, perfect-match, unique probe sets. The RMA algorithm was used for probe set (exon-level) intensity analysis. Adjustments were made for GC content and probe sequence on pre-background-subtracted values. We used background correction, quantile normalization, log2 transformation, and median polishing for summarization.

Biological interpretation

Gene enrichment analysis was used to interpret the biological impact of alternative exon usage and differential expression among ISCL-4 and FVB-like littermates. Gene Ontology (GO) enrichment analysis was undertaken in Partek Genomic Suite using a chi-square test comparing the proportion of the transcript list in an ontology, to the proportion of the background list in that same ontology. Specifically, GO pathway enrichment analysis was applied to each gene set in order to identify the top functionally enriched pathway categories related to the genes significantly differentially expressed between strains.

Microarray data accession number

The data discussed in this publication have been deposited in NCBI’s Gene Expression Omnibus (Edgar *et al.*, 2002) and are accessible through GEO Series accession number GSE47706 (http://www.ncbi.nlm.nih.gov/geo/query/acc.cgi?acc=GSE47706).

Confirmational quantitative real-time PCR expression analyses

To confirm and validate select gene expression changes, we performed quantitative real-time reverse transcription polymerase chain reaction (qRT-PCR) using hippocampal RNA samples from an independent set of FVB.B6-*Sicd2*-ISCL4 and the corresponding FVB-like litttermates. For RNA isolation, naïve mice were anesthetized with Avertin and killed by decapitation. Whole brains were removed by dissection and both hippocampi rapidly dissected out on ice. Both combined hippocampi from a mouse whole brain (~50 mg) were homogenized and total RNA extracted using the RiboPure kit™ (Ambion, Austin, TX, USA) following manufacturer’s protocols. The quantity and quality of RNA was determined using a Molecular Devices SpectraMax 190 spectrophotometer (Molecular Devices, Sunnyvale,

CA, USA), and integrity was evaluated using the Bioanalyzer 2100 platform (Agilent Technologies, Santa Clara, CA, USA).

Reactions were set up for two-step reverse transcriptase polymerase chain reaction (RT-PCR). Prior to first-strand cDNA synthesis with High Capacity cDNA archive kit (Applied Biosystems, Foster City, CA, USA), aliquots of mRNA were treated with DNase at 37°C for 30 min to eliminate potential contaminating genomic DNA. qRT-PCR was carried out using SYBR Green chemistry and the ABI Prism 7300 sequence detection system (Applied Biosystems, Foster City, CA, USA).

Primer sequences for candidate genes were designed from the sequence in the coding region of the gene; when possible, at least 1 primer spanned an exon/intron boundary using Primer 3 (Rozen & Skaletsky, 2000) based on the murine sequence obtained from the Ensembl genome browser (release 38). The specificity of each pair of primers was confirmed by its dissociation curve in quantitative real-time PCR. To correct for run-to-run variability and differences in primer efficiency, a fivefold serial dilution (ranging from 0.64 to 80 ng) of genomic DNA were included in each experiment to generate a standard curve of each candidate gene. All primer sets were tested for optimal dissociation curves with amplification efficiencies between 85 and 100%. Any primer sets not meeting these standards were redesigned.

Relative expression was measured using the relative standard curve method, which gives highly accurate quantitative results and requires the least amount of validation (Applied Biosystems, Grand Island, NY, USA). Two control reactions were run for each RNA preparation: (1) a reverse transcription and PCR reaction with no added RNA to control for contamination of the reagents; and (2) a PCR reaction without the reverse transcription reaction to detect DNA contamination of the RNA preparation. To correct for sample-to-sample variation, an endogenous control (GAPDH) was amplified with the target and served as an internal reference to normalize the data. GAPDH expression did not vary significantly across the samples, allowing it to be used as the normalizer. For relative quantification of expression of each gene between the FVB-like littermates and FVB.B6-*Sicd2*-ISCL4 strains, the comparative cycle number threshold (C_T) method ($\Delta\Delta C_T$) was used: $\Delta C_T = C_T$ (gene of interest) − C_T (reference gene), and this value calculated for each sample. The comparative $\Delta\Delta C_T$ calculation involves finding the difference between each sample's ΔC_T and the mean ΔC_T for the FVB.B6-*Sicd2*-ISCL4 strain. These values were then transformed to absolute values with a formula in which comparative expression level = $2^{-\Delta\Delta CT}$.

Statistical analysis

SigmaStat (Jandel Scientific, San Rafael, CA, USA) was used for all statistical tests. Data were presented as mean ± SEM, and differences between groups were compared statistically by one way ANOVA. One-way ANOVA with Student–Newman–Keul's *post hoc* multiple comparison test was used to assess all ISCLs for significant reduction in the extent of cell damage relative to FVB-like littermates. Mean values are given for phenotypes ± SEM. Data were considered to be statistically significant when $P < 0.05$.

Results

Fine mapping of Sicd2 through creation of interval-specific congenic lines

As previously described (Schauwecker, 2011), the ISCL were detected by screening for recombination between the flanking markers used to construct the congenic lines. All four ISCL lines that were validated as carrying unique recombination events and derived from the original FVB.B6-*Sicd2* congenic strain are shown in Figure 1. Some additional lines

were lost due to infertility. The genetic markers used to characterize each ISCL are shown, together with their mB positions. Genetic markers throughout the B6 donor region were characterized in each ISCL.

Seizure parameters following systemic administration of kainate

As susceptibility to seizure-induced cell death can be modulated by the duration and severity of seizure induction (Berger *et al.*, 1986; Ferraro *et al.*, 1995; Galanopoulou *et al.*, 2002; Holmes, 2002), we examined whether significant differences in seizure severity, the latency to the onset of the first severe seizure or the duration of severe seizures differed significantly among ISCL congenic strains and FVB-like littermates. Results for latency to first seizure and seizure duration following kainate (KA) administration for the four subcongenic lines are presented in Table 1. As depicted in Table 1, the latency to the onset of the first severe seizure differed significantly as tested by ANOVA among all ISCL congenic strains and FVB-like littermates ($F4,134 = 10.738$, $P < 0.001$). In particular, a reduction by nearly 50% was observed amongst all three ISCL strains with regard to shortened latency to the onset of severe seizures, as compared to the FVB-like littermates. Similarly, while ISCL-1 and ISCL-3 showed a trend towards increased duration of severe seizures, only ISCL-4 showed a significant increase in the duration of severe seizures as compared to FVB-like littermates ($F4,134 = 12.972$, $P < 0.001$). In contrast, it is important to note that, irrespective of mouse strain or line, observed seizures were of a similar intensity (Table 1).

Susceptibility to kainate-induced cell death in interval-specific congenic lines of Sicd2

We developed 4 interval-specific congenic lines for our *Sicd2* QTL. Sections from each of four groups of ISCL mice sacrificed 7 days following kainate injection and processed for cresyl violet staining and NeuN immunofluorescence are shown in Figure 2. Briefly, while we observed a significant protective effect amongst all four ISCL strains when cell death was assessed throughout the whole hippocampus (Figure 3A), as compared with FVB-like littermates, when cell damage was assessed across hippocampal subfields a different pattern emerged. In particular, a significant protective effect was observed in all four ISCL strains throughout area CA3, as evidenced by retention of cresyl violet staining and NeuN immunofluorescence. In contrast, we saw a significant protective effect within the dentate hilus in ISCL-2 and ISCL-4 as well, while we did not observe such a protective effect in either FVB.B6-*Sicd2* congenic mice or the other two ISCL lines (Figure 2). Moreover, only ISCL-4 demonstrated a protective effect against seizure-induced cell death in area CA1 as well.

Consistent with previous studies in mice (Schauwecker & Steward, 1997; Schauwecker *et al.*, 2000; Schauwecker, 2000, 2002a, 2002b), administration of KA to FVB-like littermates mice led to the degeneration and loss of CA3 pyramidal neurons and hilar neurons, and sporadic loss of CA1 pyramidal neurons. In accordance with previous studies (Nadler & Cuthbertson, 1980; Nadler *et al.*, 1980; Sperk *et al.*, 1983; Ben-Ari *et al.*, 1984), cells within the dentate granule cell layer and area CA2 of Ammon's horn were spared. In contrast, all ISCL strains demonstrated significantly less cell death, compared with their respective FVB-like littermates (Figure 3A). Quantitative analysis of hippocampal subfield group means revealed that ISCL-2 mice lost on average 20% fewer hilar neurons while ISCL-4 mice lost on average 40% fewer hilar neurons as compared to FVB-like littermates (Figure 3B). Within area CA3, while all ISCLs showed a reduction in the extent of cell loss as compared to FVB-like littermates. ISCL-3 showed a 55% loss of CA3 pyramidal neurons, ISCL-1 showed a 40% loss, and ISCL-2 and ISCL-4 showed the greatest protective effect with losses of only 20% or 10%, respectively. Furthermore, only ISCL-4 was protected against any cell loss within area CA1, and displayed nearly complete protection against seizure-induced excitotoxic cell loss (Figure 3). As ISCL-4 demonstrated the most significant

reduction in seizure-induced cell death and demonstrated reduced cell death in all hippocampal subfields, we chose this strain to conduct a transcriptome analysis on as compared to the FVB-like littermates.

Quality Control of RNA and Microarray Samples

Assessment of RNA integrity on the Agilent Bioanalyser 2100 indicated an average RNA Integrity Number (RIN) of 9.5, thus RNA samples provided for the microarray were of high quality. The expression data was entered into Partek® Genomics Suite™ where quality control analyses were performed. Principal Components Analysis (PCA) mapping indicated that the greatest variation between hippocampal samples was due to genotype, i.e. between ISCL-4 and FVB-like littermate samples). There was no obvious clustering based on RNA extraction date. No samples were identified as biological or technical outliers, therefore all samples were included in the subsequent bioinformatic analysis.

Hippocampal gene expression changes in Sicd2 subcongenic mice versus FVB-like littermates

To investigate the effect of strain on gene expression in the hippocampus, we analyzed hippocampal RNA using a microarray platform that utilizes multiple probes along the different exons of each gene (Affymetrix GeneChip Mouse Exon 1.0 ST array). The Affymetrix Exon 1.0 ST microarray contains 1.2 million probe sets that cover 1 million exon clusters, with an average of 40 probes per gene. The annotations used to design these probe sets are derived from a variety of sources and vary dramatically in the strength of experimental evidence which supports their existence. These annotations are divided, in order of decreasing quality of experimental support into “core”, “extended”, “full”, “free”, and “ambiguous” annotations. Our analysis was restricted to the approximately 2.2×10^5 core probe sets on the exon array. These probe sets interrogate exons derived from Ref Seq transcripts and/or full length Gen Bank mRNAs. Eight chips were analyzed per strain group, with RNA for each chip sample derived individually from the whole hippocampi of eight ISCL-4 male mice and their FVB-like littermates at 6–8 weeks of age.

To identify underlying gene expression differences between ISCL-4 and FVB-like littermate hippocampi, a one-way Analysis of Variance (ANOVA) of samples only was conducted (with genotype as factor) for those genes differentially expressed by a log fold change (LFC) $> \pm 1.2$ in response to strain. Overall, a total of 723 genes were differentially expressed between control ISCL-4 and FVB-like littermates; 157 genes had a decreased expression in ISCL-4 compared to FVB-like littermate hippocampi, while 536 had an increased expression. Of these, only four genes were located within the introgressed region on Chr 15 and all four of these genes were up-regulated in ISCL-4 mice as compared to FVB-like littermates (Table 2).

To address the question of whether abnormal splicing events are a cause or a consequence of strain-related differences in seizure-induced cell death, we carried out an exon-specific microarray experiment on both strains and assessed alternative splicing using the Partek® Genomics Suite™ program. Of the 28,072 genes with evidence of expression, 1098 genes were predicted to have at least one alternative exon in the differentiation between *Sicd2*-ISCL4 mice and FVB-like littermates. Ten of these were located in the reduced *Sicd2*-ISCL4 region (Table 3), and all of these transcripts were up-regulated in ISCL-4 mice as compared to FVB-like littermates.

Functionally enriched pathways

Genes that were differentially expressed at $p<0.05$ across the contrast of strain were imported into Partek® Genomics Suite™ and subjected to analysis with GO functional

terms. Table 4 shows the top functionally enriched pathway categories related to genes differentially expressed between FVB-like and ISCL-4 strains. Gene count refers to the number of genes from the data sets that contribute to each functional category. The p-value represents the statistical significance of each functionally enriched category identified.

Functional validation of divergently expressed genes

We selected a subset of 7 genes for confirmation of the microarray results and to obtain an independent measurement of fold changes between ISCLs and controls, based on known or predicted function. For these analyses, we used hippocampal RNA from an independent set of ISCL-4 and FVB-like littermate controls for qRT PCR. As shown in Figure 4, we confirmed upregulation of four of these genes (Enpp2: $F=10.573$; $P=0.006$; Oxr1: $F=5.512$; $P=0.034$; Rspo2: $F=50.066$; $P<0.001$; Trhr: $F=12.189$; $P=0.004$) and downregulation of one (Ttc35: $F=5.512$; $P=0.034$) by qRT-PCR analysis in hippocampal homogenates of *Sicd2*-ISCL4 mice as compared to FVB-like littermates. Four of these genes, Enpp2, Oxr1, Rspo2, and Trhr, were validated with the microarray results being concordant to the qPCR data in terms of direction of fold changes. The gene with the largest upregulation in ISCL-4 compared with FVB-like littermates as determined by qRT-PCR was Rspo2 with a 6.4 fold increase.

Discussion

We have found that susceptibility to seizure-induced excitotoxic cell death occurs in many inbred strains of mice and often differs in extent among strains due to genetic background. In particular, FVB mice experience significantly more seizure-induced cell death than B6. This differential sensitivity is explained by genes present in quantitative trait loci (QTL) on Chromosomes 18, 15, and 4 (listed in order of strength of influence on the phenotype; Schauwecker *et al.*, 2004). Prior studies (Schauwecker, 2011) had demonstrated that congenic mice expressing a B6-derived locus on the Chr. 15 region, *Sicd2*, showed reduced susceptibility to seizure-induced excitotoxic cell death following kainate administration, suggesting that the *Sicd2* interval harbors gene(s) conferring protection against seizure-induced cell death. Interval-specific congenic lines (ISCL) that encompass *Sicd2* on Chr. 15 were generated and used to fine-map this QTL.

ISCL-4 mice of the FVB.B6-*Sicd2* congenic strain show reduced seizure-induced cell death following systemic kainate administration

In the present study, we produced four interval-specific congenic lines, ISCL1-4, carrying differing intervals from Chr. 15 of B6 on an FVB-derived susceptible background. All of these subcongenic strains had decreased susceptibility compared with their FVB-like littermates, when cell damage was assessed by regional analysis of hippocampal subfields, owing to the effect of B6 alleles on Chr. 15. However, differences in the extent of hippocampal cell death were noted among the ISCL strains. When cell damage was assessed across all hippocampal subfields, only ISCL-4 showed significant protection against cell loss in all 3 hippocampal subfields (dentate hilus, area CA3 and area CA1).

Interestingly, earlier studies have suggested that reduced susceptibility to seizure-induced cell death could result from a reduction in seizure activity (Berger *et al.*, 1986; Ferraro *et al.*, 1995; Galanopoulou *et al.*, 2002; Holmes; 2002; Sucholmelova *et al.*, 2006). Thus, we examined several seizure parameters in these four ISCLstrains, such as seizure severity, seizure latency and seizure duration. Despite the dramatic protective effect we observed in ISCL-4 mice with regard to susceptibility to seizure-induced cell death in comparison to the FVB-wildtype strain, we observed a significant reduction in the latency to the first seizure and a significant increase in seizure duration. Typically, reductions in seizure latency and

increases in seizure duration suggest increased seizure sensitivity/susceptibility with resultant increases in cell death. However, we found a considerable discrepancy within the ISCL-4 mice. Although we would have expected increased cell death, as a result of the decreased seizure latency and increased seizure duration, we instead found increased protection against seizure-induced cell death. The shortened latency and increased duration of seizures give emphasis to the fact that ISCL-4 mice may actually have enhanced kainate seizure sensitivity. Nevertheless, it is important to note that although ISCL-4 show enhanced protection against susceptibility to seizure-induced cell death, these protective effects are not the result of diminished seizure sensitivity.

As differences in the extent of cell death across hippocampal subfields could result from differences in gene composition within each interval, we were guided by our working hypothesis that genes that are differentially regulated between strains and are localized to the QTL are good candidate genes to explain the differential sensitivity. In order to characterize susceptibility loci on *Sicd2* using existing subcongenic strains (Schauwecker, 2011) and identify compelling candidate genes, we undertook an integrative genomic strategy of assessing exon transcript abundance in a newly developed Chr. 15 subcongenic line.

Identifying candidate modifier genes through transcriptional profiling

As the most dramatic reduction in seizure-induced cell death susceptibility was expressed in ISCL-4, which carries a reduced B6-derived region of Chr. 15 on an FVB-derived susceptible background, we chose to examine gene expression in this subcongenic strain and compare it to gene expression in FVB-like littermate controls. We hypothesized that the phenotypic differences displayed by these mice in response to kainate can partly be explained by a different gene expression profile between the mouse strains, and that this approach could lead to the identification of candidate genes affecting susceptibility to seizure-induced cell death. As a first step in the identification of possible positional candidates for *Sicd2*, we carried out transcript profiling with microarrays to compare the level of expression of all genes in the interval in normal hippocampus from susceptible vs. ISCL mice.

Several studies have employed linkage analysis with QTL mapping to identify genomic regions regulating quantitative traits in mice (Lang *et al.*, 2010; Samocha *et al.*, 2010; Hessel *et al.*, 2012; Smolock *et al.*, 2012). However, identification of the genetic polymorphisms responsible for disease susceptibility has been a slow process. We combined fine mapping through the creation of interval specific congenic lines and expression profiling, a strategy that has been successful at identifying putative quantitative candidate genes in mice (Chiu *et al.*, 2007; Hofstetter *et al.*, 2008; Kim *et al.*, 2009; Villmann *et al.*, 2009; Kumar *et al.*, 2010). The 14.24-Mb interval that defines the ISCL-4 *Sicd2* interval on Chr. 15 contains approximately 63 known or predicted genes. Thus, using the combined approach of fine-mapping and focusing on one small region (~ 14 Mb of chromosome 15) with transcriptomics dramatically decreases the number of genes that are expected to be differentially expressed - giving us a manageable number of candidates. We determined that 90% of known genes in this region are represented on the Affymetrix GeneChip Mouse Exon 1.0 ST array chip. This allows us to identify candidate quantitative trait genes (QTGs) for the cell death susceptibility phenotype. Furthermore, because the two strains are identical except for a region on the chromosome, the *a priori* expectation is that the genes within the QTL interval that differ in expression are by definition cis-regulated (Vadasz *et al.*, 2007; Ma *et al.*, 2008; Wang *et al.*, 2010; Leduc *et al.*, 2011) and thus QTG candidates. By focusing on the region that differs, we were able to detect differences in the expression of nine cis-regulated genes. We confirmed upregulation of four of these genes, Enpp2, Oxr1,

Rspo2 and Trhr, by qRT-PCR analysis in hippocampal homogenates of *Sicd2*-ISCL4 mice as compared to FVB-like littermate mice.

Candidate modifier genes involved in seizure-induced cell death

The implicated genes have a variety of functions. Enpp2 (autotaxin) is one of the members of a group of widely conserved family of ectonucleotidases that plays a primary role in purine signaling regulation by hydrolyzing AMP to adenosine (Vuaden *et al.*, 2012). Thus, the ENPP family is involved in the generation, breakdown, and recycling of extracellular nucleotides (Bollen *et al.*, 2000; Stefan *et al.*, 2006). Since a single mutation in the mouse Enpp2 catalytic site leads to an inactive enzyme and renders homozygous knock-out mice embryonic lethal, the enzymatic activity of Enpp2 is critical to normal development (Ferry *et al.*, 2007). ENPP2 has been suggested to be involved in cell survival, proliferation, and tumor cell motility based on its ability to generate lysophosphatidic acid (LPA) (Stefan *et al.*, 2005; Van Meeteren & Moolenaar, 2007). LPA is a lipid mediator that has wide-ranging roles in cell proliferation, migration and survival (Anliker & Chun, 2004; Birgbauer & Chun, 2006; Van Meeteren & Moolenaar, 2007).

Orexins (hypocretins) are recently discovered excitatory neuropeptides synthesized mainly by neurons located in the posterolateral hypothalamus. They are involved in the regulation of neurohormones and pituitary hormone secretion, as well as in the control of cardiovascular and sleep-wake function (Hungs & Mignot, 2001; Willie *et al.*, 2001). The two types of orexins, orexin A and orexin B, mediate their effects by binding to two G-protein coupled orexin receptors, Oxr1 and Oxr2 (Langmead *et al.*, 2004). Studies have shown that loss of either orexin A or B or the receptors results in a loss of appetite as compared to littermates and a sleep disorder similar to human narcolepsy (Chemeilli *et al.*, 1999). Activation of orexin receptors can stimulate intracellular calcium influx through a number of intracellular signaling cascades (Holmqvist *et al.*, 2005; Lund *et al.*, 2000). Studies have demonstrated that Oxr1 is induced under oxidative stress (Elliott & Volkert, 2004; Natoli *et al.*, 2008), and that loss of Oxr1 causes cell death while increased protein levels can protect against oxidative stress (Oliver *et al.*, 2011). Importantly, Oliver *et al.* (2011) has shown that the sensitivity of neurons to exogenous stress can be exquisitely controlled by the level of Oxr1 expression.

R-spondins comprise a family of four secreted proteins that activate WNT/β-catenin signaling at the receptor level, leading to β-catenin-dependent gene activation (Kazanskaya *et al.*, 2004; Kim *et al.*, 2005; Nam *et al.*, 2006; Wei *et al.*, 2007). They have been shown to be novel regulators of cell proliferation, cell fate determination, and organogenesis, particularly as mutations in particular Rspo genes cause human syndromes specified by specific birth defects. Mice lacking a functional Rspo2 gene exhibit craniofacial abnormalities likely due to disrupted WNT/β-catenin signaling and gene expression within the first branchial arch (Jin *et al.*, 2011).

Thyrotropin releasing hormone, Trh, is a tripeptide hormone originally identified in hypothalamic neurons (Boler *et al.*, 1969) and secreted into the hypothalamic-hypophyseal portal blood. Trh binds to cell surface thyrotropin-releasing hormone receptors, Trhrs, which are seven transmembrane spanning receptors located on thyrotrophs and mammotrophs in the anterior pituitary gland. Binding of Trh to Trhr activates the G proteins, Gq/G11 resulting in the activation of phospholipase C and a subsequent increase in intracellular free calcium, and the release of both thyroid-stimulating hormone (TSH) and prolactin (Cook *et al.*, 2003). Thus, tight regulation of the TRHR signal is necessary for proper thyroid function. While, at present, none of these genes has been shown to play a relevant role in modulating neuronal excitability on its own, the identification of new and/or novel genes is a strength of QTL mapping in that it is location-based/hypothesis free and therefore has a

higher potential of identifying novel mechanisms related to seizure-induced cell death susceptibility. Thus, at the present time, we cannot exclude that one or a combination of these genes play important roles in cellular signaling pathways, and thus, might be involved subsequently at some level in modulating susceptibility to seizure-induced excitotoxic cell death.

It is important to note that this study is not without limitations. Advances in high-throughput gene expression platforms have enabled genome-wide analysis of gene expression, allowing investigation of both cis and trans effects. Based on our experimental design of the congenic microarray in which we focused on examining those differentially expressed genes in the donor region, we have focused primarily on annotated genes likely to be under cis regulation within the limits of the congenic interval. It is possible that our identification of any cis-regulated genes may show bias towards causal association with respect to transcript abundance. In particular, a proportion of the total heritability of gene expression could be explained by the effects of trans regulatory variants introgressed in the given congenic strain and these trans variants could be critical to differences in gene expression observed between our subcongenic strain and FVB-like littermates.

Conclusions

In this study, we have demonstrated that changes in alternative splicing occurred between our ISCL-4 and background strain of FVB-like littermates. Our results highlight the benefit of using transcriptomics in addition to fine mapping via construction of ISCL lines to identify QTGs. Thus, we propose that Enpp2, Oxr1, Rspo2, and Trhr are likely candidates in the respective genetic region and believe that directed study will identify pathways regulated during epilepsy, giving further insight into differences in the pathological consequences of seizures. These genes likely contribute to susceptibility to seizure-induced cell death and its consequences regardless of the mechanistic origin of increased susceptibility. Compared to other approaches based on DNA microarrays that interrogate single whole genes, studying the transcriptome at the exon level provides an accurate detailed knowledge about the variations occurring within the genes. Further functional characterization of gene regions alternatively spliced has the potential to improve the understanding of the complicated biological processes connecting isoform variations and phenotype variations. Lastly, an optimal test to prove that a candidate gene is causal for the QTL effect is quantitative complementation (Peruzzi *et al.*, 2009; Villmann *et al.*, 2009; Kerr *et al.*, 2012), which requires knockout models in particular genetic backgrounds. Therefore, the approach of developing novel subcongenic lines with ever smaller donor segments combined with bioinformatics, sequence, expression, and functional analyses remains an optimal strategy to find causal sequence variation for seizure-induced cell death susceptibility candidate genes identified in this study.

Acknowledgments

The author wishes to thank Ms. Margaret Kornacki for technical assistance. This work was supported by RO1 NS38696.

Abbreviations

ANOVA	Analysis of Variance
B6	C57BL/6J
Chr. 15	Chromosome 15

EDTA	ethylenediaminetetraacetic acid
FDR	false discovery rate
FVB	FVB/NJ
ISCL	interval-specific congenic line
KA	kainic acid
qRT-PCR	quantitative real-time reverse transcription polymerase chain reaction
QTG	quantitative trait gene
QTL	quantitative trait loci
PCA	principal components analysis
RIN	RNA integrity number
SE	status epilepticus
SDS	sodium dodecyl sulfate

References

Anliker B, Chun J. Cell surface receptors in lysophospholipid signaling. Semin Cell Dev Biol. 2004; 15:457–465. [PubMed: 15271291]

Ben-Ari Y, Tremblay E, Berger M, Nitecka L. Kainic acid seizure syndrome and binding sites in developing rats. Brain Res. 1984; 316:284–288. [PubMed: 6467019]

Ben-Ari Y. Limbic seizure and brain damage produced by kainic acid: mechanisms and relevance to human temporal lobe epilepsy. Neuroscience. 1985; 14:375–403. [PubMed: 2859548]

Berger ML, Lefauconnier JM, Tremblay E, Ben-Ari Y. Limbic seizures induced by systemically applied kainic acid: how much kainic acid reaches the brain? Adv Exp Med Biol. 1986; 203:199–209. [PubMed: 2878561]

Birgbauer E, Chun J. New developments in the biological functions of lysophospholipids. Cell Mol Life Sci. 2006; 63:2695–2701. [PubMed: 16988788]

Boler J, Enzmann F, Folkers K, Bowers CY, Schally AV. The identity of chemical and hormonal properties of the thyrotopin releasing hormone and pyroglutamyl-histidyl-proline amide. Biochem Biophys Res Commun. 1969; 37:705–710. [PubMed: 4982117]

Bollen M, Gijsbers R, Ceulemans H, Stalmans W, Stefan C. Nucleotide pyrophosphatases/phosphodiesterases on the move. Crit Rev Biochem Mol Biol. 2000; 35:393–432. [PubMed: 11202013]

Chemelli RM, Willie JT, Sinton CM, Elmquist JK, Scammell T, Lee C, Richardson JA, Williams SC, Xiong Y, Kisanuki Y, Fitch TE, Nakazato M, Hammer RE, Saper CB, Yanagisawa M. Narcolepsy in orexin knockout mice: molecular genetics of sleep regulation. Cell. 1999; 98:437–451. [PubMed: 10481909]

Chiu S, Kim K, Haus KA, Espinal GM, Millon LV, Warden CH. Identification of positional candidate genes for body weight and adiposity in subcongenic mice. Physiol Genomics. 2007; 31:75–85. [PubMed: 17536020]

Cook LB, Zhu CC, Hinkle PM. Thyrotropin-releasing hormone receptor processing: role of ubiquitination and proteasomal degradation. Mol Endocrinol. 2003; 17:1777–1791. [PubMed: 12805411]

Darvasi A. Interval-specific congenic sctrains (ICSC): an experimental design for mapping a QTL into a 1-centimorgan interval. Mamm Genome. 1997; 8:163–167. [PubMed: 9069114]

Darvasi A. Experimental strategies for the genetic dissection of complex traits in animal models. Nat Genet. 1998; 18:19–24. [PubMed: 9425894]

Edgar R, Domrachev M, Lash AE. Gene Expression Omnibus: NCBI gene expression and hybridization array data repository. Nucleic Acids Res. 2002; 30:207–210. [PubMed: 11752295]

Elliott NA, Volkert MR. Stress induction and mitochondrial localization of Oxr1 proteins in yeast and humans. Mol Cell Biol. 2004; 24:3180–3187. [PubMed: 15060142]

Ferraro TN, Golden GT, Smith GG, Berrettini WH. Differential susceptibility to seizures induced by systemic kainic acid treatment in mature DBA/2J and C57BL/6J mice. Epilepsia. 1995; 36:301–307. [PubMed: 7614915]

Ferry G, Giganti A, Cogé F, Bertaux F, Thiam K, Boutin JA. Functional invalidation of the autotaxin gene by a single amino acid mutation in mouse is lethal. FEBS Lett. 2007; 581:3572–3578. [PubMed: 17628547]

Franklin, KBJ.; Paxinos, G. The Mouse Brain in Stereotaxic Coordinates. Academic Press; New York: 1997.

Fujikawa DG, Daniels AH, Kim JS. The competitive NMDA receptor antagonist CGP 40116 protects against status epilepticus-induced neuronal damage. Epilepsy Res. 1994; 17:207–219. [PubMed: 7912191]

Fujikawa DG. Neuroprotective effect of ketamine administered after status epilepticus onset. Epilepsia. 1995; 36:543–558. [PubMed: 7555966]

Fujikawa DG. The temporal evolution of neuronal damage from pilocarpine-induced status epilepticus. Brain Res. 1996; 725:11–22. [PubMed: 8828581]

Galanopoulou AS, Vidaurre J, Moshe SL. under what circumstances can seizures produce hippocampal injury: evidence for age-specific effects. Dev Neurosci. 2002; 24:355–363. [PubMed: 12640173]

Hessel EV, van Lith HA, Wolterink-Donselaar IG, de Wit M, Hendrickx DA, Kas MJ, de Graan PN. Mapping an X-linked locus that influences heat-induced febrile seizures in mice. Epilepsia. 2012; 53:1399–1410. [PubMed: 22780306]

Hofstetter JR, Hitzemann RJ, Belknap JK, Walter NA, McWeeney SK, Mayeda AR. Characterization of the quantitative trait locus for haloperidol-induced catalepsy on distal mouse chromosome 1. Genes Brain Behav. 2008; 7:214–223. [PubMed: 17696997]

Holmes GL. Seizure-induced neuronal injury: animal data. Neurology. 2002; 59:S3–S6. [PubMed: 12428025]

Holmqvist T, Johansson L, Ostman M, Ammoun S, Akerman KE, Kukkonen JP. OX1 orexin receptors couple to adenylyl cyclase regulation via multiple mechanisms. J Biol Chem. 2005; 280:6570–6579. [PubMed: 15611118]

Hungs M, Mignot E. Hypocretin/orexin, sleep and narcolepsy. Bioessays. 2001; 23:397–408. [PubMed: 11340621]

Jin YR, Turcotte TJ, Crocker AL, Han XH, Yoon JK. The canonical Wnt signaling activator, R-spondin2, regulates craniofacial patterning and morphogenesis within the branchial arch through ectodermal-mesenchymal interaction. Dev Biol. 2011; 352:1–13. [PubMed: 21237142]

Kazanskaya O, Glinka A, del Barco Barrantes I, Stannek P, Niehrs C, Wu W. R-spondin2 is a secreted activator of Wnt/beta-catenin signaling and is required for Xenopus myogenesis. Dev Cell. 2004; 7:525–534. [PubMed: 15469841]

Kerr B, Soto CJ, Saez M, Abrams A, Walz K, Young JI. Transgenic complementation of MeCP2 deficiency: phenotypic rescue of Mecp2-null mice by isoform-specific transgenes. Eur J Hum Genet. 2012; 20:69–76. [PubMed: 21829232]

Kim KA, Kakitani M, Zhao J, Oshima T, Tang T, Binnerts M, Liu Y, Boyle B, Park E, Emtage P, Funk WD, Tomizuka K. Mitogenic influence of human R-spondin1 on the intestinal epithelium. Science. 2005; 309:1256–1259. [PubMed: 16109882]

Kim S, Zhang S, Choi KH, Reister R, Do C, Baykiz AF, Gershenfeld HK. An E3 ubiquitin ligase, Really Interesting New Gene (RING) Finger 41, is a candidate gene for anxiety-like behavior and beta-carboline-induced seizures. Biol Psychiatry. 2009; 65:425–431. [PubMed: 18986647]

Kong S, Lorenzana A, Deng Q, McNeill TH, Schauwecker PE. Variation in Galr1 expression determines susceptibility to excitotoxin-induced cell death in mice. Genes, Brain and Behav. 2008; 7:587–598.

Kumar KG, DiCarlo LM, Volaufova J, Zuberi AR, Richards BK. Increased physical activity cosegregates with higher intake of carbohydrate and total calories in a subcongenic mouse strain. Mamm Genome. 2010; 21:52–63. [PubMed: 20033694]

Lang DH, Gerhard GS, Griffith JW, Vogler GP, Vandenbergh DJ, Blizard DA, Stout JT, Lakoski JM, McClearn GE. Quantitative trait loci (QTL) analysis of longevity in C57BL/6J by DBA/2J (BXD) recombinant inbred mice. Aging Clin Exp Res. 2010; 22:8–19. [PubMed: 20305363]

Langmead CJ, Jerman JC, Brough SJ, Scott C, Porter RA, Herdon HJ. Characterization of the binding of [3H]-SB-674042, a novel nonpeptide antagonist, to the human orexin-1 receptor. Br J Pharmacol. 2004; 141:340–346. [PubMed: 14691055]

Leduc MS, Hageman RS, Verdugo RA, Tsaih SW, Walsh K, Churchill GA, Paigen B. Integration of QTL and bioinformatics tools to identify candidate genes for triglycerides in mice. J Lipid Res. 2011; 52:1672–1682. [PubMed: 21622629]

Lorenzana A, Chancer Z, Schauwecker PE. A quantitative trait locus on chromosome 18 is a critical determinant of excitotoxic cell death susceptibility. Eur J Neurosci. 2007; 25:1998–2008. [PubMed: 17439488]

Lund PE, Shariatmadari R, Uustare A, Detheux M, Parmentier M, Kukkonen JP, Akerman KE. The orexin OX1 receptor activates a novel Ca2+ influx pathway necessary for coupling to phospholipase C. J Biol Chem. 2000; 275:30806–30812. [PubMed: 10880509]

McKhann GM, Wenzel HJ, Robbins CA, Sosunov AA, Schwartzkroin PA. Mouse strain differences in kainic acid sensitivity, seizure behavior, mortality, and hippocampal pathology. Neuroscience. 2003; 122:551–561. [PubMed: 14614919]

Ma Q, Chirn GW, Szustakowski JD, Bakhtiarova A, Kosinski PA, Kemp D, Nirmala N. Uncovering mechanisms of transcriptional regulations by systematic mining of cis regulatory elements with gene expression profiles. BioData Min. 2008; 1:1–4. [PubMed: 18822148]

Miller SA, Dykes DD, Polesky HF. A simple salting out procedure for extracting DNA from human nucleated cells. Nucl Acids Res. 1988; 16:1215. [PubMed: 3344216]

Müller CJ, Gröticke I, Hoffmann K, Schughart K, Löscher W. Differences in sensitivity to the convulsant pilocarpine in substrains and sublines of C57BL/6 mice. Genes Brain Behav. 2009; 8:481–492. [PubMed: 19493016]

Nadler JV, Cuthbertson GJ. Kainic acid neurotoxicity toward hippocampal formation: dependence on specific excitatory pathways. Brain Res. 1980; 195:47–56. [PubMed: 6249441]

Nadler JV, Perry BW, Gentry C, Cotman CW. Degeneration of hippocampal CA3 pyramidal cells induced by intraventricular kainic acid. J Comp Neurol. 1980; 192:333–359. [PubMed: 7400401]

Nam JS, Turcotte TJ, Smith PF, Choi S, Yoon JK. Mouse cristin/R-spondin family proteins are novel ligands for the Frizzled 8 and LRP6 receptors and activate beta-catenin-dependent gene expression. J Biol Chem. 2006; 281:13247–13257. [PubMed: 16543246]

Natoli R, Provis J, Valter K, Stone J. Expression and role of the early-response gene Oxr1 in the hyperoxia-challenged mouse retina. Invest Ophthamol Vis Sci. 2008; 49:4561–4567.

Oliver PL, Finelli MJ, Edwards B, Bitoun E, Butts DL, Becker EBE, Cheeseman MT, Davies B, Davies KE. Oxr1 is essential for protection against oxidative stress-induced neurodegeneration. PLoS Genetics. 2011; 7:e1002338. [PubMed: 22028674]

Peruzzi PP, Lawler SE, Senior SL, Dmitrieva N, Edster PA, Gianni D, Chiocca EA, Wade-Martins R. Physiological transgene regulation and functional complementation of a neurological disease gene deficiency in neurons. Mol Ther. 2009; 17:1517–1526. [PubMed: 19352323]

Racine RJ. Modification of seizure activity electrical stimulation. II Motor seizure. Electroencephalogr Clin Neurophysiol. 1972; 32:281–294. [PubMed: 4110397]

Rozen, S.; Skaletsky, HJ. Primer3 on the WWW for general users and for biologist programmers. In: Krawetz, S.; Misener, S., editors. Bioinformatics Methods and Protocols: Methods in Molecular Biology. Humana Press; Totowa, N.J: 2000. p. 365-386.

Samocha KE, Lim JE, Cheng R, Sokoloff G, Palmer AA. Fine mapping of QTL for prepulse inhibition in LG/J and SM/J mice using F(2) and advanced intercross lines. Genes Brain Behav. 2010; 9:759–767. [PubMed: 20597988]

Schauwecker PE, Steward O. Genetic determinants of susceptibility to excitotoxic cell death: implications for gene targeting approaches. Proc Natl Acad Sci USA. 1997; 94:4103–4108. [PubMed: 9108112]

Schauwecker PE, Ramirez JJ, Steward O. Genetic dissection of the signals that induce synaptic reorganization. Exp Neurol. 2000; 161:139–152. [PubMed: 10683280]

Schauwecker PE. Seizure-induced neuronal death is associated with induction of c-Jun N-terminal kinase and is dependent on genetic background. Brain Res. 2000; 884:116–128. [PubMed: 11082493]

Schauwecker PE. Complications associated with genetic background effects in a model of experimental epilepsy. Prog Brain Res. 2002a; 135:139–148. [PubMed: 12143336]

Schauwecker PE. Modulation of cell death by mouse genotype: differential vulnerability to excitatory amino acid-induced lesions. Exp Neurol. 2002b; 178:219–235. [PubMed: 12504881]

Schauwecker PE, Williams RW, Santos JB. Genetic control of sensitivity to hippocampal cell death induced by kainic acid: a quantitative trait loci analysis. J Comp Neurol. 2004; 477:96–107. [PubMed: 15281082]

Schauwecker PE. Congenic strains provide evidence that a mapped locus on chromosome 15 influences excitotoxic cell death. Genes Brain and Behav. 2011; 10:100–110.

Sidman, RL.; Angevine, JB.; Taber Pierce, E. Atlas of the Mouse Brain and Spinal Cord. Harvard University Press; Cambridge, MA: 1971.

Smolock EM, Ilyushkina IA, Ghazalpour A, Gerloff J, Murashev AN, Lusis AJ, Korshunov VA. Genetic locus on mouse chromosome 7 controls elevated heart rate. Physiol Genomics. 2012; 44:689–698. [PubMed: 22589454]

Sousa N, Madeira MD, Paula-Barbosa MM. Effects of corticosterone treatment and rehabilitation on the hippocampal formation of neonatal and adult rats. An unbiased stereological study. Brain Res. 1998; 794:199–210. [PubMed: 9622630]

Sperk G, Lassmann H, Baran H, Kish SJ, Seitelberger F, Hornykiesicz O. Kainic acid induced seizures: neurochemical and histopathological changes. Neuroscience. 1983; 10:1301–1315. [PubMed: 6141539]

Sperk G. Kainic acid seizures in the rat. Prog Neurobiol. 1994; 42:1–32. [PubMed: 7480784]

Stefan C, Jansen S, Bollen M. NPP-type ectophosphodiesterases: unity in diversity. Trends Biochem Sci. 2005; 30:542–550. [PubMed: 16125936]

Stefan C, Jansen S, Bollen M. Modulation of purinergic signaling by NPP-type ectophosphodiesterases. Purinergic Signal. 2006; 2:361–370. [PubMed: 18404476]

Suchomelova L, Baldwin RA, Kubova H, Thompson KW, Sankar R, Wasterlain CG. Treatment of experimental status epilepticus in immature rats: dissociation between anticonvulsant and antiepileptogenic effects. Pediatr Res. 2006; 59:237–243. [PubMed: 16439585]

Vadasz C, Smiley JF, Figarsky K, Saito M, Toth R, Gyetvai BM, Oros M, Kovacs KK, Mohan P, Wang R. Mesencephalic dopamine neuron number and tyrosine hydroxylase content: Genetic control and candidate genes. Neuroscience. 2007; 149:561–572. [PubMed: 17920205]

Van Meeteren LA, Moolenaar WH. Regulation and biological activities of the autotaxin-LPA axis. Prog Lipid Res. 2007; 46:145–160. [PubMed: 17459484]

Villmann C, Oertel J, Ma-Högemeier ZL, Hollmann M, Sprengel R, Becker K, Breitinger HG, Becker CM. Functional complementation of Glra1 (spd-ot), a glycine receptor subunit mutant, by independently expressed C-terminal domains. J Neurosci. 2009; 29:2440–2452. [PubMed: 19244519]

Vuaden FC, Savio LE, Ramos DB, Casali EA, Bogo MR, Bonan CD. Endotoxin-induced effects on nucleotide catabolism in mouse kidney. Eur J Pharmacol. 2012; 674:422–429. [PubMed: 22108548]

Wang H, Liu Y, Briesemann M, Yan J. Computational analysis of gene regulation in animal sleep deprivation. Physiol Genomics. 2010; 42:427–436. [PubMed: 20501693]

Wei Q, Yokota C, Semenov MV, Doble B, Woodgett J, He X. R-spondin 1 is a high affinity ligand for LRP6 and induces LRP6 phosphorylation and beta-catenin signaling. J Biol Chem. 2007; 282:15903–15911. [PubMed: 17400545]

West MJ, Slomianka L, Gundersen HJ. Unbiased stereological estimation of the total number of neurons in the subdivisions of the rat hippocampus using the optical fractionator. Anat Rec. 1991; 231:482–497. [PubMed: 1793176]

Willie JT, Chemelli RM, Sinton CM, Yanagisawa M. To eat or to sleep? Orexin in the regulation of feeding and wakefulness. Annu Rev Neurosci. 2001; 24:429–458. [PubMed: 11283317]

Winawer MR, Makarenko N, McCloskey DP, Hintz TM, Nair N, Palmer AA, Scharfman HE. Acute and chronic responses to the convulsant pilocarpine in DBA/2J and A/J mice. Neuroscience. 2007; 149:465–475. [PubMed: 17904758]

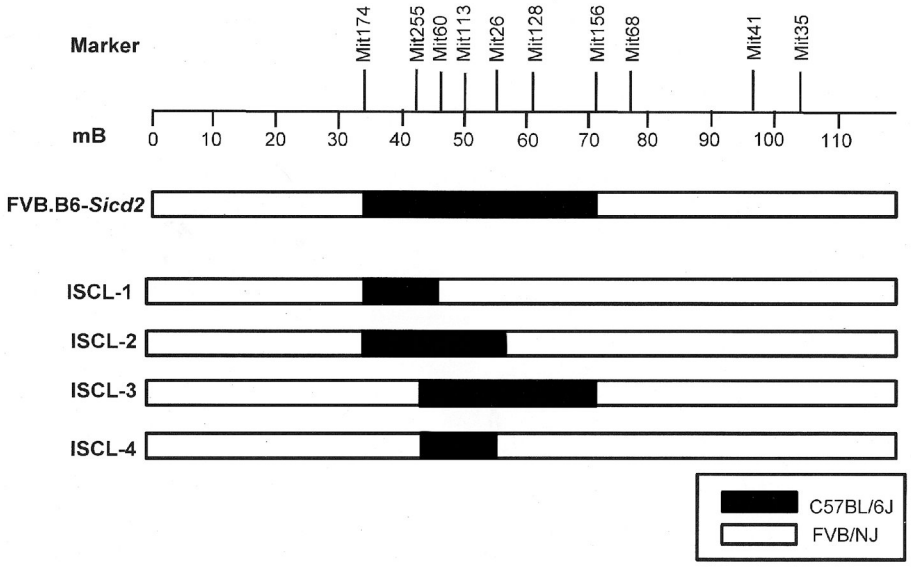

FIG. 1.

Fine-mapping of *Sicd2* on Chr. 15 with interval-specific congenic lines. ISCLs with varying B6-derived Chr. 15 segments as compared to the FVB.B6-*Sicd2* congenic strain. The B6-derived interval is shown in black, and white denotes the interval containing the recipient, FVB strain. Strains were produced as described in Materials and Methods. Microsatellite DNA markers used for selective specific recombinants are shown at the top and numbers below refer to the genetic map position in megabases (http://www.informatics.jax.org/).

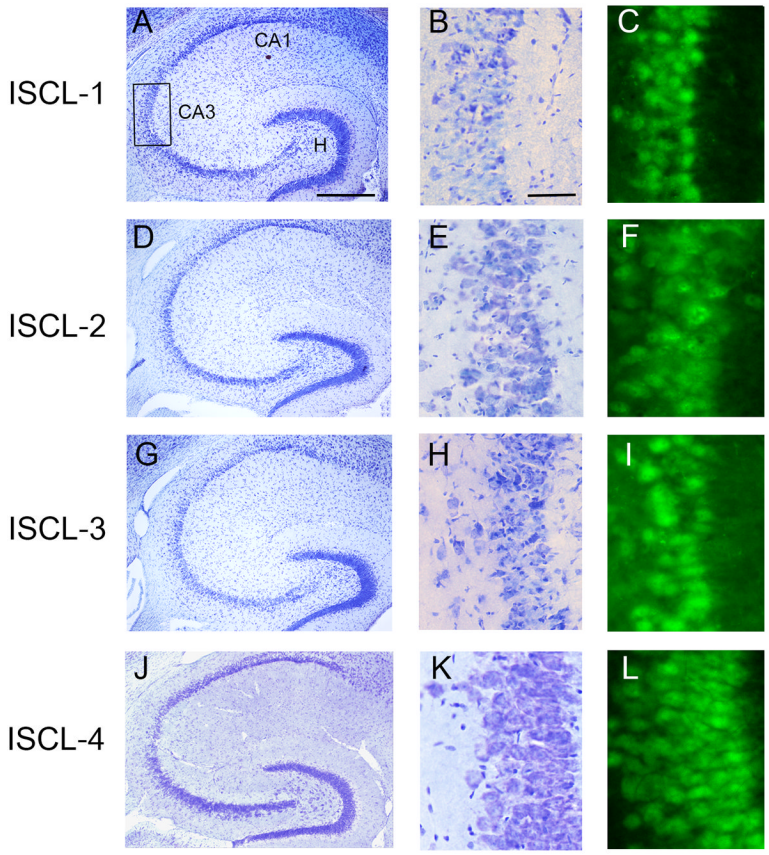

FIG. 2.

Comparison of susceptibility to kainate-induced cell death in four interval-specific congenic lines (ISCL). Four interval-specific congenic lines [interval-specific congenic lines (ISCLs)-1-4] were developed and tested to attain higher resolution mapping of seizure-induced cell death (*Sicd2*). Lines were produced as described in Materials and Methods. Low-magnification photomicrographs (A,D,G,J) of cresyl violet-stained stained horizontal sections of the hippocampus illustrating surviving cells throughout the hippocampus 7 days following systemic kainate administration. High-magnification cresyl violet (B,E,H,K) and NeuN-immunofluorescent stained (C,F,I,L) horizontal sections of area CA3 among the four groups. Note that little to no cell death was observed in ISCL-4 throughout all hippocampal subfields (J, K,L). CA1 and CA3, hippocampal subfields; H, dentate hilus. High-magnification photomicrographs represent details of the boxed area of CA3 shown in A. Scale bar: 750 μm (A,D,G,J) and 100 μm (B,C,E,F,H,I,K,L).

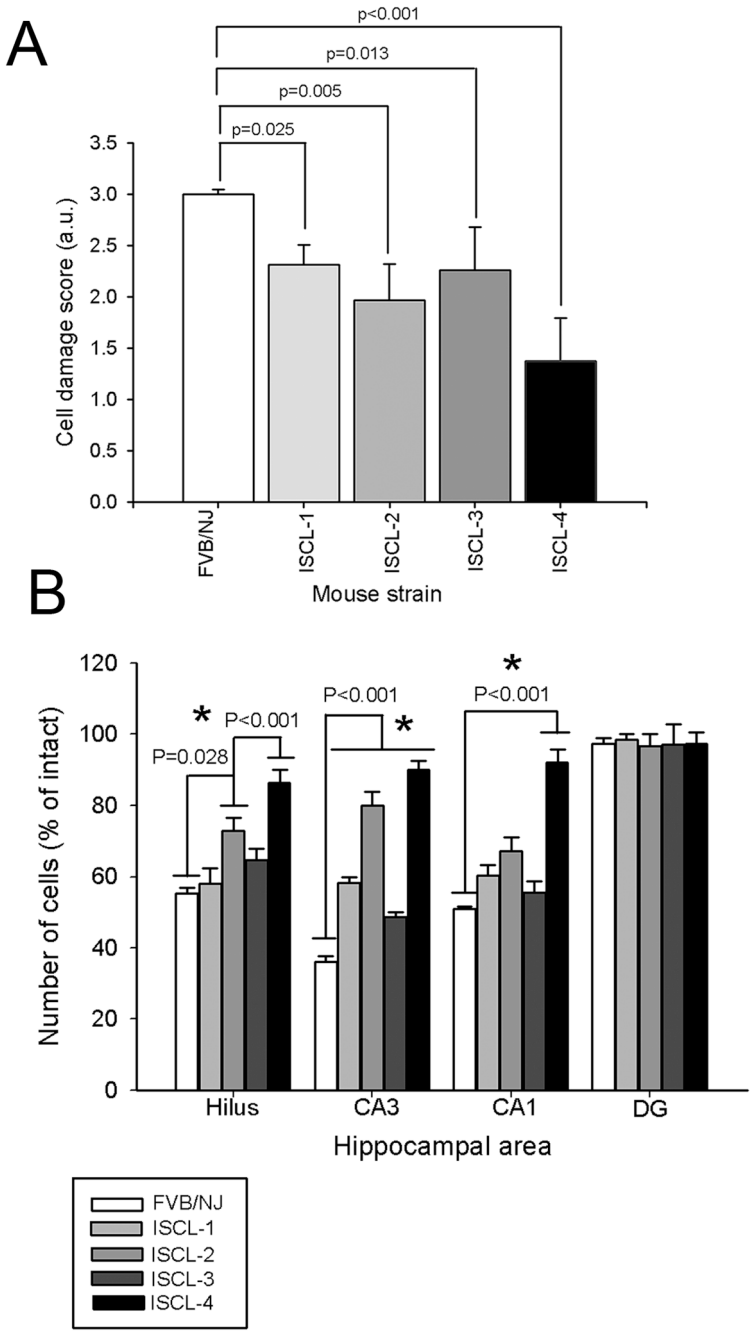

FIG. 3.

Kainate-induced cell death susceptibility phenotype of four interval-specific congenic lines as compared to FVB-like littermates. A. Data represent neuronal damage scores (in arbitrary units, mean ± S.E.M.) for FVB.B6-*Sicd2*-ISCL 1–4 and FVB-like littermates. The extent of neuronal damage was indexed using a histological damage score. B. Quantitative analysis of neuronal density in hippocampal subfields following KA administration to ISCLs 1–4 and FVB-like littermates. Strain-dependent differences in cell loss in hippocampal subfields were observed at 7 days following KA administration. Viable surviving neurons were estimated by cresyl violet staining. Bars denote the percentage of surviving neurons (as compared with saline-injected sham control FVB-like littermates). Data represent the mean

± SEM for at least 9 mice per strain. Note that cell loss amongst all 3 hippocampal subfields was only reduced in ISCL-4.

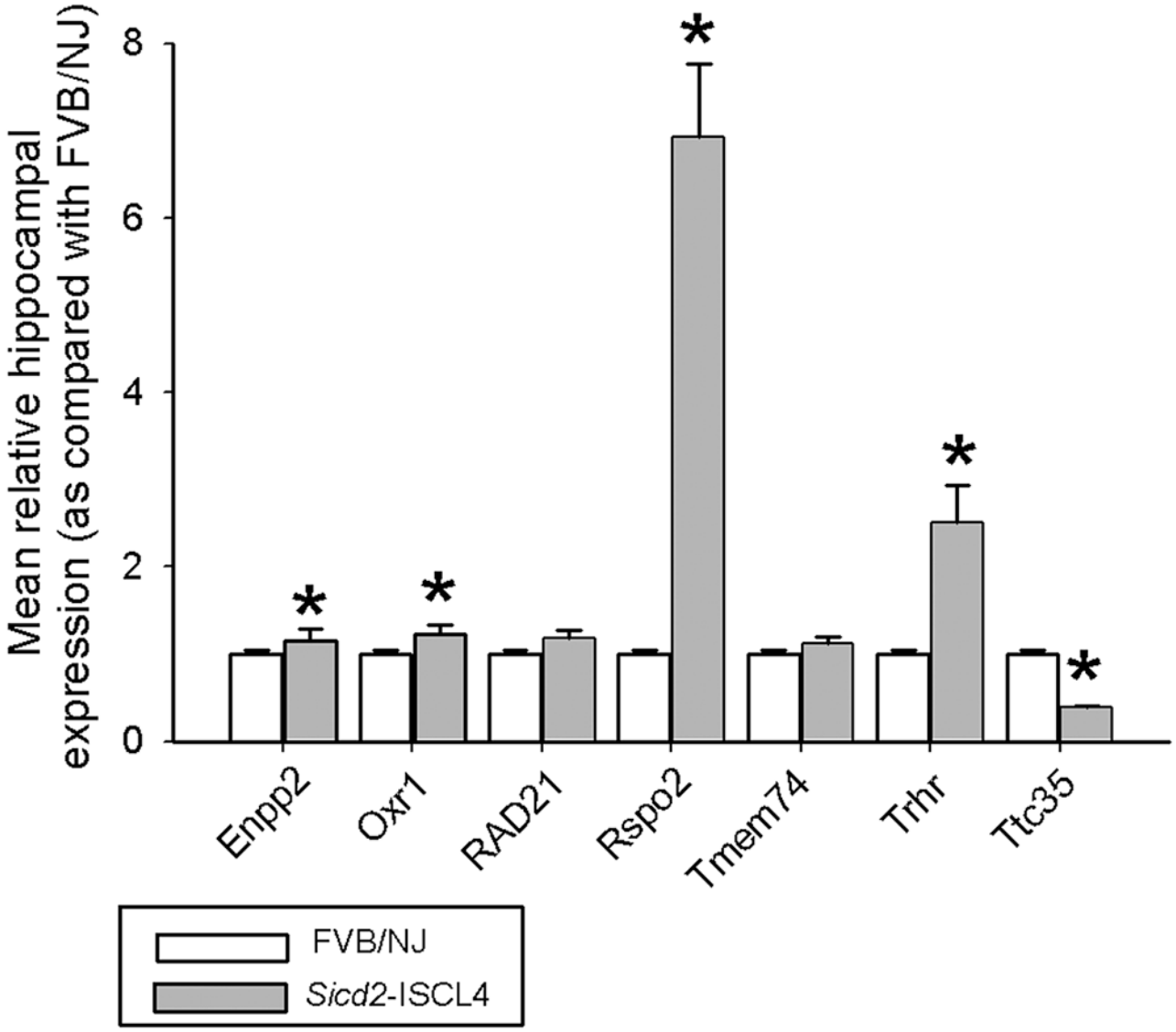

FIG. 4.

Quantitative real-time PCR validation of differentially expressed genes located within the FVB.B6-*Sicd2*-ISCL4 donor region. Quantitative real-time PCR expression of seven candidate genes in hippocampus of FVB.B6-*Sicd2*-ISCL-4 as compared with FVB-like littermates. Expression levels were standardized relative to GAPDH transcript levels using the standard curve method. Values are provided as mean ± SEM from 8 mice per strain analyzed in triplicate. Four alternatively regulated genes (Enpp2, Oxr1, Rspo2, and Trhr) confirmed the exon microarray results. *P<0.05.

Table 1

Effect of kainic acid administration on seizure parameters in FVB-like littermates and interval-specific recombinant strains of the FVB.B6-*Sicd2* congenic mice

Mouse line	Stages 1–4 (% of mice)	Stage 5 (% of mice)	Latency (min)	Duration (min)
FVB-like littermates (n=14)	100 ± 0	95.9 ± 0.79	62.9 ± 3.3	71.4 ± 6.3
ISCL-1 (n=37)	100 ± 0	94.9 ± 1.19	35.5 ± 2.5[a]	90.8 ± 4.2
ISCL-2 (n=29)	100 ± 0	92.6 ± 0.83	39.6 ± 3.9[a]	57.0 ± 4.7
ISCL-3 (n=45)	100 ± 0	99.1 ± 1.03	33.8 ± 2.2[a]	93.2 ± 4.0
ISCL-4 (n=14)	100 ± 0	93.4 ± 0.69	24.4 ± 3.2[a]	120.3 ± 18.0[b]

KA induced a similar level of stage irrespective of mouse line. A significant difference in latency to onset of stage 4 seizures was observed among all ISCL mice ([a]$F_{4,131}=10.74$; $P<0.001$) and a significant difference in duration of stage 4/5 seizures was observed in ISCL-4 mice as compared to FVB-like littermates ([b]$F_{4,131}=12.97$; $P<0.001$). Data are represented as mean ± S.E.M.

Eur J Neurosci. Author manuscript; available in PMC 2014 January 07.

Table 2

Chromosome 15 genes differentially expressed in FVB-like littermates and ISCL-4 hippocampal samples (P<0.05, fold change > ±1.2)

Gene name	Gene symbol	RefSeq	p value	Fold change (to FVB-like)
R-spondin 2 homolog	Rspo2	NM_172815	4.49×10^{-5}	−1.24726
Thryotropin releasing hormone	Trhr	NM_013696	3.28×10^{-5}	−1.57712
Angiopoietin 1	Angpt1	ENSMUST 22921	1.75×10^{-4}	−1.27947
Tumor necrosis factor receptor	Tnfrsf11b	NM_008764	1.00×10^{-3}	−1.24346

P values were determined by ANOVA between the mean values of FVB-like and ISCL-4 normalized for signal intensities. The fold change is the relative level of expression in the FVB-like and ISCL-4 mice measured as a ratio of normalized signal spot intensities of FVB/ISCL-4 (ISCL-4 up-regulated) or ISCL-4/FVB (ISCL-4 down-regulated).

Table 3

Chromosome 15 transcripts exhibiting a significant interaction of strain (ISCL-4 vs. FVB-like) in the hippocampus

Gene symbol	Gene product	Reference Sequence	Transcript cluster ID	Probe sets (n)	Alt-splice[a] score	Fold change
Enpp2	Ectonucleotide pyrophophatase	NM_015744.2	6835759	28	3.53×10^{-58}	1.17192
Rad21	RAD21 homolog (S. pombe)	NM_009009	6835640	17	9.99×10^{-19}	−1.04023
Rspo2	R-spondin 2 homolog	NM_172815	6835372	14	5.12×10^{-18}	−1.24726
Tmem74	Transmembrane protein 74	NM_175502	6835403	6	6.64×10^{-14}	1.00867
Ttc35	Tetratricopeptide repeat domain 35	NM_025736	6830131	5	1.66×10^{-13}	−1.13097
Oxr1	Oxidation resistance 1	NM_001130166	6830055	20	8.55×10^{-6}	1.01434
Nudcd1	NudC domain containing 1	NM_026149	6835415	16	1.19×10^{-4}	1.0938
Trhr	Thyrotropin releasing hormone receptor	NM_013696	6830154	5	1.29×10^{-3}	−1.57712
A930017MO1Rik	Smg-5 homolog	NR_033609	6830174	12	1.50×10^{-3}	1.14331
Sybu	Syntabulin (syntaxin-interacting)	NM_178765	6835428	11	3.90×10^{-3}	−1.08361

[a]Rows are sorted by alt-splice score in ascending order.

Table 4

Functional Annotation Analysis of Genes Differentially Regulated by strain in the hippocampus/Comparison of Sicd2-ISCL4 and FVB-like littermate hippocampi: gene ontology groups over-represented in list of differentially expressed genes

Function or Type of Protein Group	No. Genes in Cluster	P-value[a]
Positive regulation of intracellular protein kinase cascade	6	6.75×10^{-7}
Thyrotropin-releasing hormone receptor activity	2	2.84×10^{-5}
Positive regulation of platelet-derived growth factor production	2	1.68×10^{-5}
L-aminoadipate-semialdehyde dehydrogenase activity	2	1.11×10^{-4}
Positive regulation of cholesterol biosynthetic process	6	1.10×10^{-4}
Rhythmic behavior	2	4.08×10^{-3}
Olfactory learning	3	1.53×10^{-3}
Positive regulation of p38MAPK cascade	2	2.93×10^{-2}
Negative regulation of protein glycosylation in Golgi	2	1.25×10^{-2}

The Functional Annotation tool examined a list of genes with a fold change of ± 1.2 and a P value of <0.05.

[a]P values were determined by Fisher exact test.